CMT Ceramics in Modern Technologies
Techna Group srl

Copyright © Techna Group S.r.l., Faenza, Italy

Spark Plasma Sintering of Combustion Synthesized TiB_2-Si Composite

Le Liu[a], Sofiya Aydinyan[a]*, Tatevik Minasyan[a], Janis Baronins[a], Maksim Antonov[a], Suren Kharatyan[b], Irina Hussainova[a, c]
[a]Tallinn University of Technology, Tallinn, Estonia; [b]A.B. Nalbandyan Institute of Chemical Physics NAS RA, Yerevan, Armenia; [c]ITMO University, St. Petersburg, Russian Federation

Titanium diboride-silicon composite was fabricated by innovative method of self-propagating high-temperature synthesis (SHS) from the mixtures of titanium, magnesium dodecaboride and silicon in constant pressure reactor in argon atmosphere at 0.5-2 MPa pressure. The key influence of initial mixture composition, sample geometry and external gas pressure on the combustion features, products phases and microstructure characteristics were examined. Direct fabrication of fully dense TiB_2-(30-44)wt.%Si composite with improved physico-mechanical properties was performed using spark plasma sintering (SPS) at a relatively low temperatures (1250-1350 °C) with a dwelling time of 3 min at pressure of 50 MPa. Erosive wear behavior of the composites was studied both at room and elevated temperatures. The highest erosion resistance against silica particles impact was demonstrated by composite with the lowest silicon content.

Keywords: Spark plasma sintering; TiB_2-Si composites; Combustion synthesis; Mechanical properties; Microstructure; Erosion.

1. Introduction

Titanium diboride (TiB_2) as one of the extremely hard and chemically stable ceramic materials with metallic conductivity and high corrosion resistance is considered as a potential candidate for cutting tools, electric devices, self-draining inert cathodes in aluminium electrolysis cells and many other fields of industry demanding materials for high temperature structural and wear-resistant applications [1-6]. Among numerous promising properties of TiB_2 there are high melting point (3225 °C), relatively low density (4.5 $g \cdot cm^{-3}$), high hardness (25 GPa) and Young's modulus (510 - 575 GPa), combined with remarkable high-temperature strength [1,6]. Neutron absorption capability of boron makes TiB_2 one of the best choices for control rod material exploited in high temperature nuclear reactors. Much wider application of this material is inhibited by poor sinterability due to a low self-diffusion coefficient, an exaggerated grain growth at high temperature, and formation of oxide layer on the surface of particles combined with a low fracture tolerance of the final product [1,2,4,7-9]. Fast anisotropic grain growth produces high internal stresses resulting in the onset of spontaneous severe microcracking during cooling from sintering temperatures. In order to meet this threat, a new generation of materials, namely multi-element composite materials with titanium diboride as a constituent element, are expected to be developed. Binderless TiB_2 can traditionally be densified at temperatures over ~2100 °C generally assisted by a high pressure during sintering. Wang et al. have prepared TiB_2 ceramic of nearly full density by hot pressing at 1900 °C under 30 MPa pressure [10]. Konigshofer et al. have reported densities as high as 99.9% by hot pressing at high temperature 1800 °C and 45 MPa pressure [11]. Improvement in densification conditions of TiB_2 can be achieved by liquid phase sintering with metallic additives such as Ni, Cr, Fe, etc. [12-15]. Particular attention was being paid to Al [14], Cu or Fe as a toughening binder [16-18] attempting to get systems with a high specific modulus. However, the presence of a metallic binder leads to degradation in some mechanical properties of TiB_2-based cermets especially at a high temperature. The non-metallic additives can be used to improve sinterability without deterioration of boride's properties.

Recently, hard titanium boride-based ceramic thin films alloyed with silicon (Si) have been attracted continuing research attention in attempt to take the advantage of excellent wear and high-temperature oxidation resistance (up to 1000 °C), which are particularly important for cutting tool applications [1,19]. It was shown that alloying of transition-metal boride coatings with Si reduces crystallinity and/or promotes a nanocrystalline structure to improve thermal stability and oxidation resistance [20]. Composite of TiB_2 and Si promotes the high protective performance combined with the structural strength giving an optimum combination of hardness and ductility.

TiB_2 based ceramics can be prepared by carbothermic reduction of mixed oxides of boron and titanium, reduction of titanium oxide by boron carbide and carbon, reduction of mixed oxides by metals like aluminium, silicon, magnesium, etc., electrochemical synthesis, sol-gel and solid state reactions, or synthesis from the elements by heating or mechanical alloying [21-24]. The application of high temperatures, the long reaction times and the use of complicated equipment are the main restrictions for an efficient fabrication of TiB_2 based powders. Self-propagating high-temperature synthesis (SHS) designated as an alternative energy-saving method for the large scale production of many compounds, particularly TiB_2 based composites [25,26]. SHS has a number of advantages over other approaches, such as low energy consumption, high efficiency, simple processing and

* *Corresponding author*
E-mail address: sofiya.aydinyan@ttu.ee

https://doi.org/10.29272/cmt.2018.0009
Received September 7, 2018; Received in revised form October 18, 2018; Accepted October 19, 2018

equipment, and no need for extra processing to obtain product with controlled particle size and distribution to be able ready for sintering. For the preparation of TiB_2-Si composite by SHS, a highly exothermic combustion reaction can be performed in the Ti-B-Si mixture, and the reaction propagates in a self-sustaining manner by utilizing the thermal energy released from the combustion reaction of elementary powders. However, there is still a lack of knowledge on determination of optimum and reliable sintering parameters of combustion synthesized TiB_2/Si powders.

The sinterability of TiB_2/Si is the key issue for its technical application and is also limited by purity and particle size, which play a crucial role during sintering. On the other hand, to the best of our knowledge, the reports concerning the sintering of combustion synthesized TiB_2/Si ceramics using SPS technique are absent.

This study focuses on the preparation of TiB_2-Si composite powder by SHS method from the exothermic Ti-MgB_{12}-Si mixture and addresses the issue of relatively low temperature spark plasma sintering (SPS) of TiB_2-Si composite material. SHS process optimization based on both thermodynamic consideration and experimental procedure enables to obtain the product with tailored granulometric composition and purity.

2. Experimental

2.1. Materials preparation by SHS

The precursors are listed in Table 1. Magnesium dodecaboride was used as a widely available source of boron. The green mixture of reactants was homogenized in a ceramic mortar for 15 minutes, and the cylindrical samples with 2.1-2.3 $g \cdot cm^{-3}$ density, height of 30-35 mm, 20 mm in diameter were prepared by uniaxial pressing of 50 kN. Two C-type tungsten-rhenium thermocouples (wire diameter 0.2 mm) previously covered with a thin layer of boron nitride were placed into holes drilled beforehand in each sample to record temperature-time profiles of the combustion process.

The prepared samples were positioned in a reaction chamber CPR-3l. The reactor was sealed, evacuated, purged with argon (purity 99.97%, oxygen content less than 0.02%) and filled with Ar to the pressure of 0.5-2 MPa. For the synthesis of pilot batches, a tubular reactor (CPR-3.5l) was exploited. To initiate the combustion reaction, the short-term annealing of tungsten coil (12 V, 1-2 s) positioned on the upper surface of a sample was employed. The maximum combustion temperature (T_c) for each sample was calculated as an average of maxima for two temperature profiles. The average value of combustion velocity is calculated by the following formula: $U_c = L \cdot t^{-1}$, where L - the distance between the thermocouples, t - the time distance between the thermocouple's signals. The standard error of measurement for T_c and U_c were ± 20 °C and 5%, respectively. The combustion process was followed by crushing of the specimens into powders for further densification by SPS.

2.2. SPS processing

To prepare the powder for SPS sintering, the SHS synthesized TiB_2-Si composite material was ball milled for 30 min at a fixed rotation speed of 200 rpm using ZrO_2 grinding media and the ball-to-powder weight ratio of 3:1. Subsequently the powder was sieved through a 60-mesh screen and green shaped to 45 mm-pellet by linear pressing at 20 MPa. The composite powder was spark plasma sintered (KCE®-FCT HP D 10-GB, FCT Systeme GmbH, Germany) in vacuum ($5 \cdot 10^{-2}$ mbar) at temperatures of 1250, 1300 and 1350 °C with simultaneous application of 10-50 MPa (3-16 kN) pressure for a dwell time of 3 min. The heating rate employed was 100 $°C \cdot min^{-1}$ for ramp-up and the cooling rate was set up to ~200 $°C \cdot min^{-1}$.

Table 1. Characteristics of precursors.

No	Precursor	Particle size, μm	Mark	Purity, %
1	Ti	<40	PTM	>99
2	B	<1	B-99	99
3	Si	<20	KR0	98.8
4	MgB_{12} (magnesium dodecaboride or polyboride)	<10		>98

2.3. High-temperature abrasive-erosive wear test

Erosion testing was conducted with the help of a centrifugal four-channel accelerator described in detail elsewhere [27]. Six kilograms of silica sand with mean size of 0.3 mm was used as erodent. For brittle ceramics, the maximum wear rate during erosion is mostly observed at impact angle between 75° and 90°; in contrast, the ductile metals have the highest wear rate at low angles of solid particle impingement (usually between 10° and 45°) [28,29]. Thus, for the spark plasma sintered TiB_2-(30-40 wt.%) Si samples, the selected velocity of the particles was set to 80 $m \cdot s^{-1}$ at the impact angle 30°. Tests were performed successively at room temperature, 550 and 650 °C. The erosion rate was determined as volume loss of the target sample per mass of erodent particles ($mm^3 \cdot kg^{-1}$). The sample surface was polished with an abrasive paper to a surface roughness (Ra) of about 0.1 μm. To quantify the weight loss, the specimens were ultrasonically cleaned in ethanol and weighed before and after the test to the nearest 0.1 mg using GR-202 A&D Instruments balance. The tests were repeated at least three times and results were averaged.

2.4. Characterization

The density of sintered samples was measured by Archimedes technique (density kits Mettler Toledo ME204, Australia) using water as an immersion medium and phase composition was studied with the help of a Siemens Bruker D5005 X-ray analyser using a Philips X'Pert PRO diffractometer (40 mA, 40 kV, Cu Kα radiation, λ = 0.1542 nm, step size of 0.02°, PANalytical, Netherlands). Crystalline phases and their relative contents were estimated by Rietveld refinement method, which was performed by quantitative analysis of the phases detected with the corresponding XRD patterns. Microstructures and phase morphologies were examined using a field-emission scanning electronic microscope (Zeiss Evo MA15, Germany) equipped with energy dispersive spectroscopy (EDS).

The Vickers microhardness (HV) and indentation fracture toughness were measured on the polished surface using hardness tester Indentec 5030 SKV applying a load of 98.1 N for 10 s.

3. Results and discussion

3.1. Combustion

To establish suitable amount of the constituents for the preparation of the composite material, thermodynamic calculations were performed for the Ti-xMgB_{12}-ySi system in a wide range of mole amounts of MgB_{12} and Si (x, y) and an ambient gas pressure 0.5 MPa using "ISMAN-THERMO" software package [30]. The formation area for TiB_2-Si system was prescribed depending on magnesium dodecaboride (up to 1/5 mol) and silicon (changes from 0 up to 4 mol) amounts corresponding to a wide temperature zone (1200-2800 °C), Fig. 1. At a lower amount of MgB_{12} (x<2/13 mol), apart from TiB_2 and Si, titanium silicides

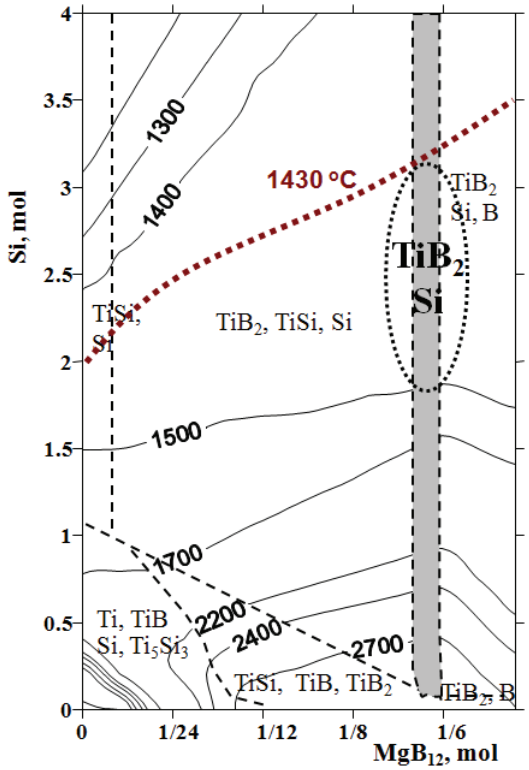

Figure 1. Thermodynamic calculations in the Ti-MgB_{12}-Si system, P=0.5 MPa.

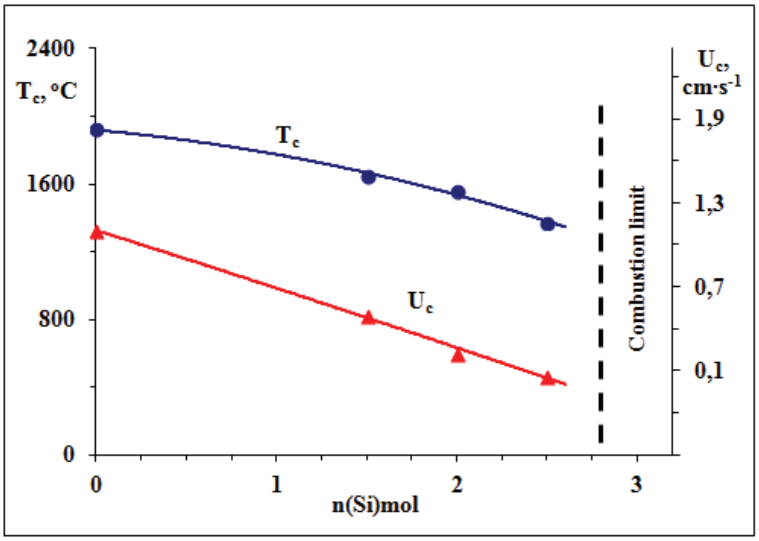

Figure 2. Combustion parameters (U_c, T_c) in the Ti+1/6MgB_{12}+***n***Si mixture depending on silicon amount (n), P(Ar)=0.5 MPa, d=20 mm, F=45 kN.

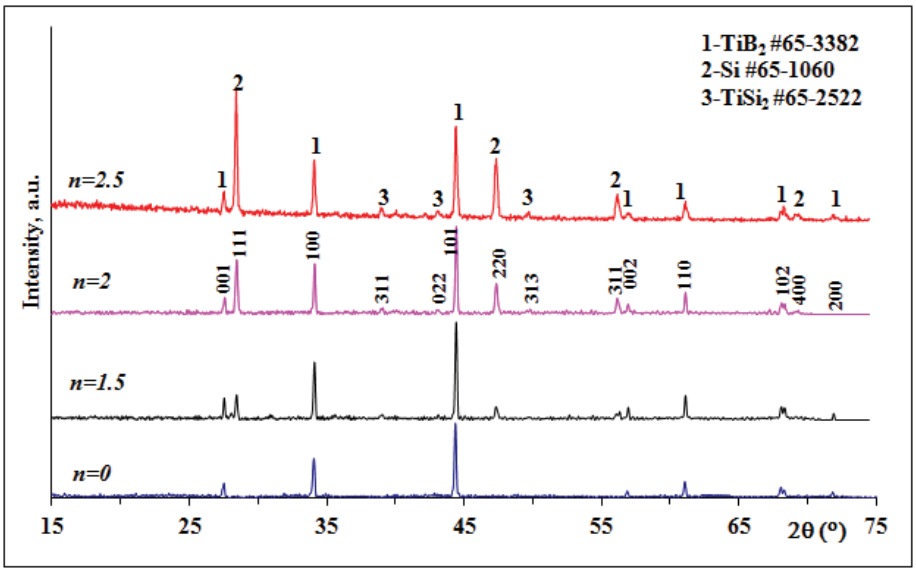

Figure 3. XRD patterns of the Ti+1/6MgB_{12}+***n***Si mixtures depending on silicon amount (n), P(Ar)=0.5 MPa.

(TiSi, Ti_5Si_3) and titanium monoboride are also present in the condensed equilibrium product. When x>1/6 mol, there is free boron remaining in the final product. In terms of preparation of TiB_2-Si composite powder, namely TiB_2 core particles covered by molten silicon, x=1/6 and y=2 moles were chosen as the optimum amounts of MgB_{12} and silicon. On the other hand, at T>1400 °C, the emergence of titanium silicides was considered as a competitive process to TiB_2 formation.

Combustion synthesis was performed based on thermodynamic calculations close to the moderate temperature area of possible TiB_2/Si formation (~1430 °C). Combustion limit was achieved at mixture with n(Si)=2.75 regardless to the ambient gas pressure (0.1-2 MPa) and the relative density of the initial specimen (30-60 wt.%).

The examination of combustion parameters for the Ti+MgB_{12}+***n***Si mixtures demonstrated that combustion temperature (T_c) and combustion velocity (U_c) were decreased with an increase of silicon amount (n) in the initial mixture. Thermal energy is consumed during silicon heating and melting, i.e. in most cases, silicon acts as an inert diluent without direct contribution to the self-sustaining combustion reaction leading to smooth decrease in U_c and T_c values, Fig. 2. At lower argon pressure (<1 MPa) $TiSi_2$ formation was observed due to titanium-silicon interaction.

XRD analysis of the combustion product of Ti+1/6MgB_{12}+***n***Si mixture evidenced the substantial effect of the amount of silicon in the initial mixture at a pressure of 0.5 MPa, Fig. 3. The final product contains titanium diboride and silicon, when n=1.5-2 moles; and trace amounts of titanium silicide, when n(Si)>2. According to the reaction stoichiometry in the presence of $TiSi_2$, some amount of free boron (amorphous) should also be present in the combustion product, which, however, was not detected by XRD analysis.

The influence of preliminary compression of the samples on the combustion parameters was insignificant; however, it manipulates the composition of the combustion product. After processing, the specimens with initial relative density Δ=35% contained TiB_2, Si, $TiSi_2$ and B. The specimens with density of above Δ>50% represented the targeted TiB_2/Si composite material.

To reveal the influence of an inert gas pressure on the combustion parameters and product composition, the combustion experiments were conducted in the Ti+1/6MgB_{12}+2Si system under 0.5-2 MPa argon pressure. Combustion wave propagated through the sample with 0.2-0.3 cm·s^{-1} average velocity at temperature of 1500-1600 °C. XRD analysis of the combustion product of Ti+1/6MgB_{12}+2Si mixture showed that increasing pressure up to P>1 MPa allows to get rid of byproducts ($TiSi_2$, B) and the combustion product contains solely titanium diboride and silicon, Fig. 4. Magnesium was not observed in the combustion products; however, the XRD analysis of condensed eliminations taken from the walls of the synthesis reactor showed the presence of some amount of Mg/MgO mixture.

The samples (m=500 g of each) were synthesized in a pilot tubular reactor at optimum 1 MPa argon pressure using Ti+1/6MgB_{12}+2Si mixture. The comparison of combustion thermograms of pilot batches (m=500 g) and small samples (m=20 g) is shown in Fig. 5. The formation of TiB_2/Si agglomerated powder at the combustion temperature near to the melting point of silicon (T_c=1420-1450 °C, U_c=0.1 cm·s^{-1}) was confirmed by XRD analysis, Fig. 6a. Post-processing milling of specimens during 30 min resulted in preparation of the powder with around 1-3 μm particle size for further densification by SPS, Fig. 6b.

Fig. 5 demonstrates that the combustion thermograms of the pilot samples, Fig. 5a, are significantly differ from the typical combustion thermograms of cylindrical samples, Fig. 5b, particularly in their heating and cooling rates (difference in order of tens) and dwelling time at a maximum temperature (about 1 min. instead of few seconds). These provide favourable conditions for the complete conversion of reagents in the combustion and the post-combustion zones for the mass production.

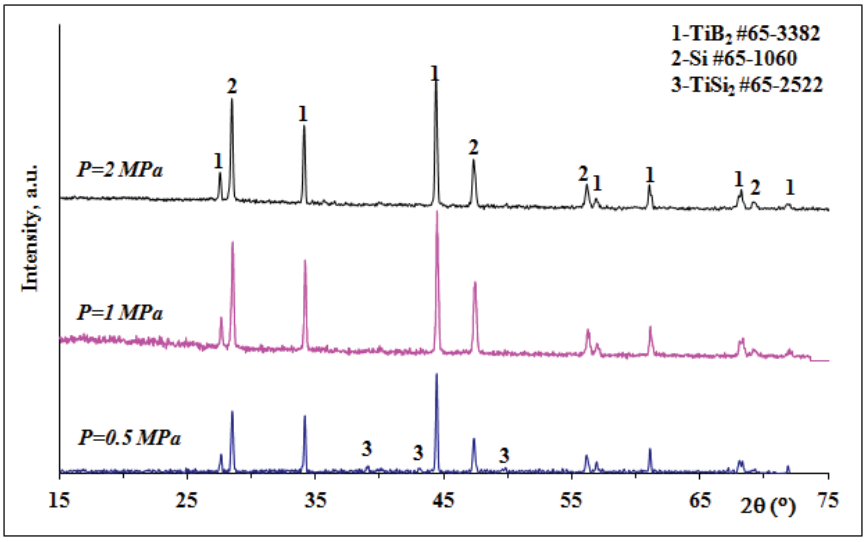

Figure 4. XRD patterns of the Ti+1/6MgB_{12}+2Si mixture vs. argon pressure.

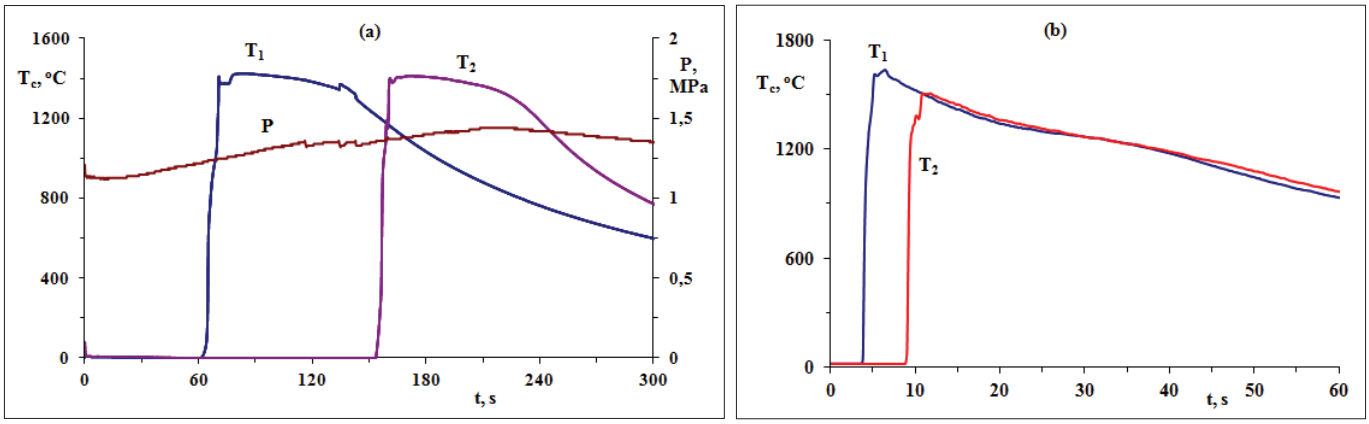

Figure 5. Combustion thermograms of the Ti+1/6MgB_{12}+2Si mixture, P(Ar) =1 MPa for the pilot batches (m=500 g, V_{h1}=20 °C·s^{-1}) (a) and small samples (m=20 g, V_{h2}=300 °C·s^{-1}) (b).

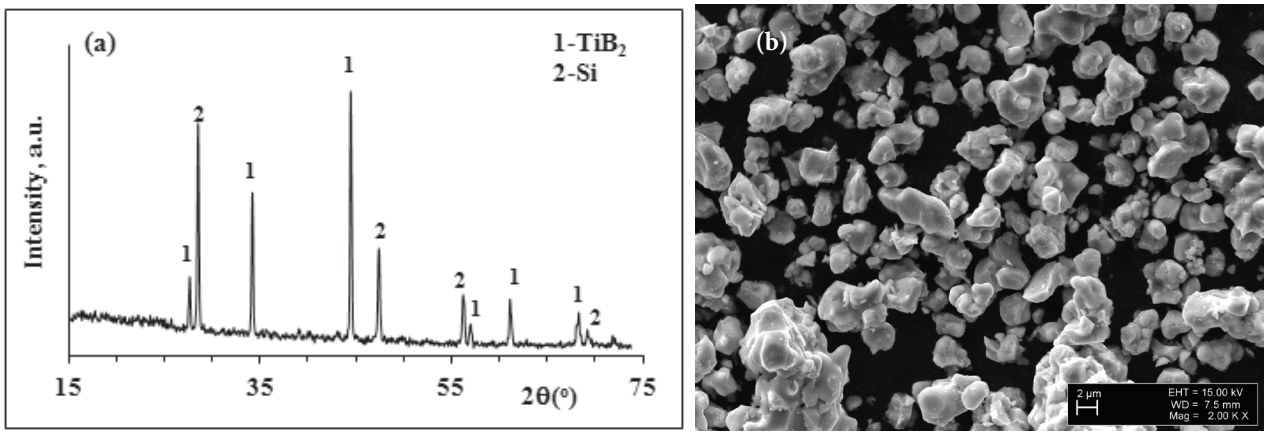

Figure 6. XRD pattern (a) and SEM image (b) of the combustion product of the Ti+1/6MgB_{12}+2Si mixture, P(Ar)=1 MPa, after milling, t=30 min, r=200 rpm.

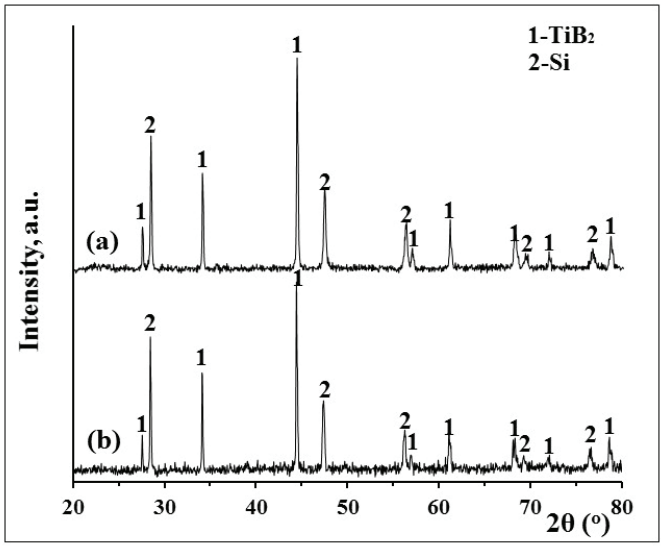

Figure 7. XRD patterns of a) SHS produced and b) SP sintered TiB_2-Si composite (1300 °C, 50 MPa).

3.2. Spark plasma sintering

3.2.1. Morphology and phase composition of spark plasma sintered samples

The microstructural analysis of the composites was performed to determine the dependence of the hardness on the microstructures. Fig. 7 displays the XRD patterns of combustion synthesized (a) and compacted (b) TiB_2/Si composite. Apparently both the XRD patterns have the same characteristic peaks of TiB_2 and Si, which asserts that there was no obvious chemical reaction between the components during the sintering procedure.

Fig. 8 compares the microstructures of the composites containing 44.0 and 30.4 wt.% of silicon and sintered at different temperatures. Microstructural analysis revealed that the TiB_2 grains in all compositions had a predominantly rounded morphology and were distributed non-homogeneously throughout the silicon matrix. Moreover, non-uniform distribution of coarse and micro-sized grains is recognizable. The sizes, calculated as an average of at least 100 grains, were of around 0.5 μm for fine grains and 3 μm for coarse ones suggesting that TiB_2 particles coalesce due to close contact during sintering. Particles of TiB_2 in the sample (c) are in a submicron range and more spherical. EDS mapping of sintered TiB_2-Si sample is demonstrated in Fig. 9.

3.2.2. Density and hardness measurements of spark plasma sintered samples

The SHS synthesized TiB_2+Si and TiB_2+2Si composite powders were sintered using graphite crucibles in a range of temperatures from 1250 to 1350 °C, which are lower than the melting points of the both constituents (T_m(Si) =1425 °C, T_m(TiB_2) =3225 °C), Table 2. Near full density was achieved for all sintered samples.

Vickers' hardness was determined from the average of at least ten indents and its values are summarized in Table 1. The hardness of TiB_2-Si composites varies from as low as 4 GPa up to 11 GPa depending on the composition (Si content), microstructure evolution, as well as sintering conditions. As it was expected, the values increased with increasing TiB_2 volume fraction and sintering temperature. The highest hardness value was recorded as 10.5 GPa for the TiB_2+Si sample sintered at 1350 °C using pressure of 50 MPa.

Fracture toughness measured by different methods gives values in the range of 3.73-5.71 MPa·$m^{1/2}$ for the TiB_2-44wt.%Si samples sintered at 1300 °C (Table 3), which is comparable with TiB_2-SiC-Si composite with representative value of 3.5 MPa·$m^{1/2}$ in fracture toughness [31].

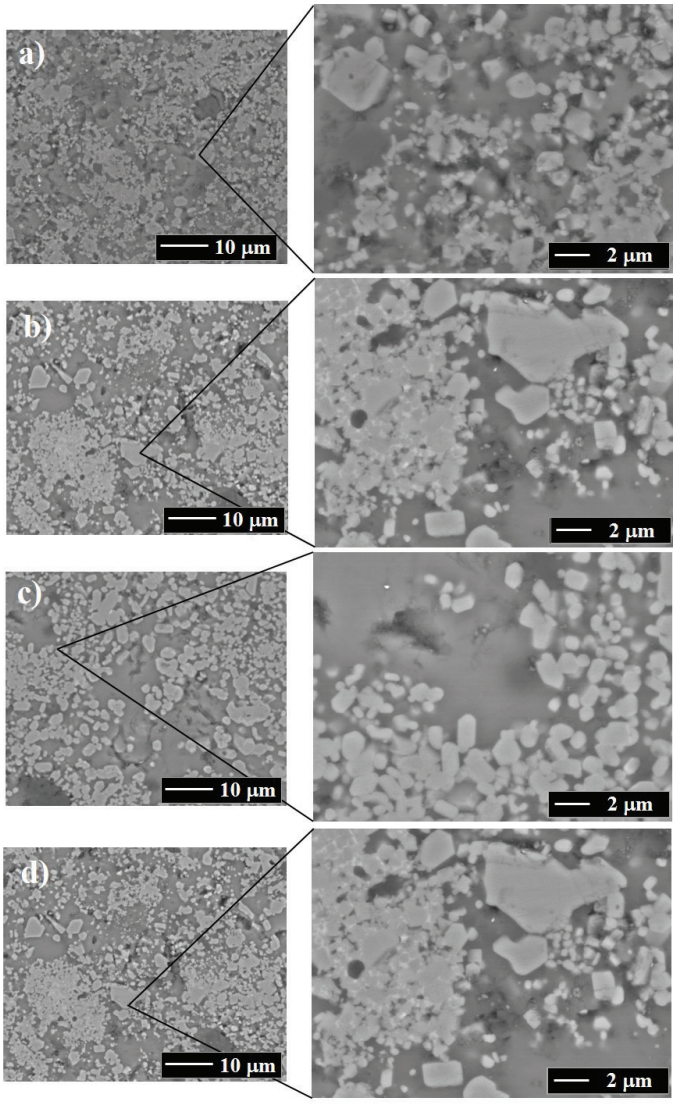

Figure 8. SEM images of samples sintered at (a) 1250 °C and 50 MPa, (b) 1300 °C and 50 MPa, (c) 1350 °C and 50 MPa, (d) 1350 °C and 10 MPa.

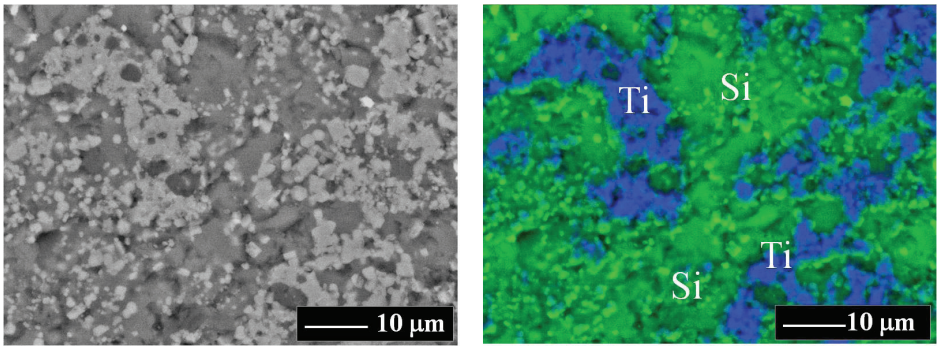

Figure 9. EDS mapping of SP-sintered sample at 1250 °C, 50 MPa (boron is not shown).

Table 2. Sintering conditions, density and hardness of SPS-ed TiB_2-Si composites.

No	Si content (wt.%) *	T, °C	Pressure, MPa	Archimedes density, g/cm³	Relative density, %	Vickers hardness, HV10, GPa
a	44.0	1250	50	3.166	99.25	4.6±0.35
b	44.0	1300	50	3.179	99.66	7.2±0.5
c	30.4	1350	50	3.475	99.00	10.5±0.5
d	44.0	1350	10	3.140	98.43	4.4±0.4

*Silicon content was determined after SPS according to Rietveld refinement method
*$\rho(TiB_2$-44wt.%Si) = 3.19 g/cm³, $\rho(TiB_2$-30wt.%Si) = 3.51 g/cm³ (calculated by $\rho = 100/(\omega_1/\rho_1+\omega_2/\rho_2)$

3.3. High-temperature erosion

Fig. 10 shows the volumetric erosive wear rate of the spark plasma sintered TiB_2/Si materials recorded during the centrifugal solid particle erosion test at impact angle of 30° and different temperatures. Despite of recordable difference in hardness, the materials containing 44% of silicon (samples *a* and *b*) demonstrate similar wear rate at temperatures of 20, 550, and 650 °C. Material with the lowest Si binder content (the silicon lean sample *c*) and expectedly with the highest hardness shows twofold higher wear resistance at both the room and elevated temperatures. The material sintered at a relatively low pressure (sample *d*) is the least erosion resistant material, which can be explained by low hardness due to recognizable porosity [32].

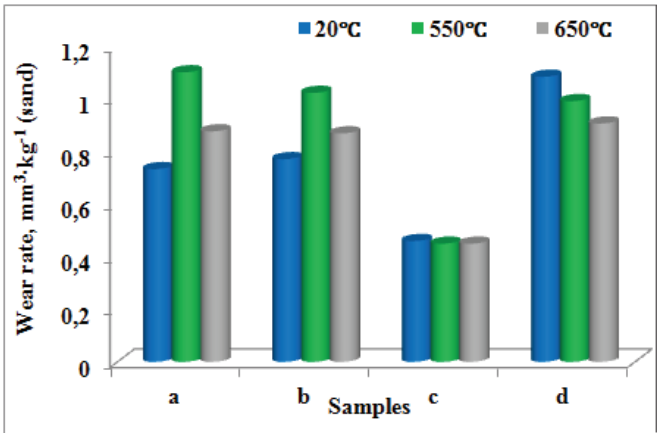

Figure 10. Wear rate of TiB_2-Si materials at different temperatures.

Table 3. Fracture toughness of the TiB_2-44wt.%Si samples.

Fracture toughness (MPa·m$^{1/2}$)		
Palmqvist	Median	Evans Method
5.71	4.62	3.73

The wear performance of TiB_2-Si is highly affected by the formation of SiO_2 protective layer developed through oxidation of a binder phase at elevated temperatures. Si-based ceramic coatings are acknowledged as one of the most effective protection systems against oxidation attributed to the formation of SiO_2 glassy thin layer of low oxygen permeability [33,34]. This fact may explain a better erosion resistance of TiB_2-Si composite at temperature of 650 °C, which is higher than the oxidation point of silicon (570 °C).

The SEM examination and EDS analysis evidence the presence of areas corresponding to the formation of SiO_2 and TiO_2 and phases containing Mg and Fe incorporated from the erodent sand, Fig. 11.

Fig. 12 displays SEM micrographs of the surfaces damaged by silica particles travelling under an impact angle of 30° at temperature 650 °C. The surfaces exposed to the impact of the erodent particles are severely damaged and deficient with the binder silicon. However, SEM images reveal no apparent difference in morphology even at relatively high magnifications (2000x). Scars of recognizable plastic deformation and TiB_2 clusters separation combined with depletion of the binder around boride result in weakening of the materials and removal of the unsupported boride. Similar mechanisms responsible for erosive wear are reported for either cemented carbides [28] or ZrC-based composites [32].

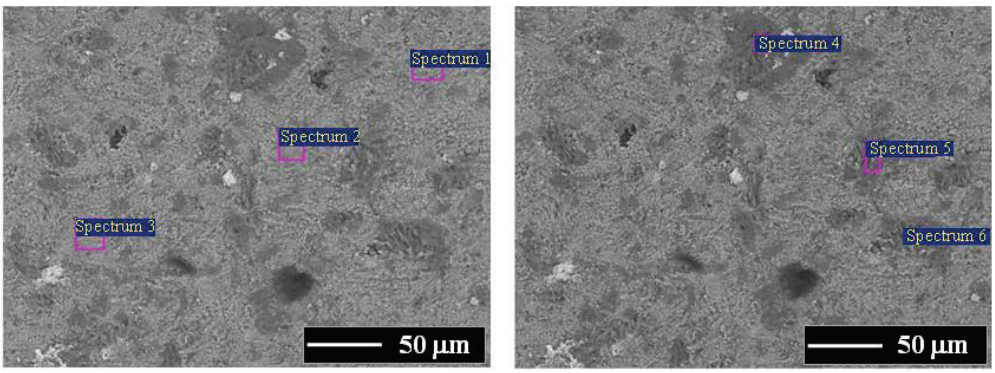

Spectrum \ Element content %	C	O	Si	Ti	Trace elements	Total
Spectrum 1	6.04	-	38.69	49.08	6.19	100.00
Spectrum 2	8.68	-	32.36	56.42	2.54	100.00
Spectrum 3	5.74	-	37.93	53.97	2.36	100.00
Spectrum 4	5.00	52.56	40.08	1.62	0.74	100.00
Spectrum 5	4.23	56.67	36.44	2.26	0.40	100.00
Spectrum 6	2.49	53.52	36.56	6.97	0.46	100.00

Figure 11. SEM images and EDS analysis of the surface of sample (a) eroded at 650 °C.

4. Conclusions

Combustion of the Ti+1/6MgB_{12}+xSi mixture under 0.5-2 MPa argon atmosphere and at temperature of 1420-1450 °C enabled the preparation of TiB_2/Si composite powder with 2 µm average particle size. Near full density titanium diboride-silicon compacts from combustion synthesized TiB_2/Si powders were prepared by

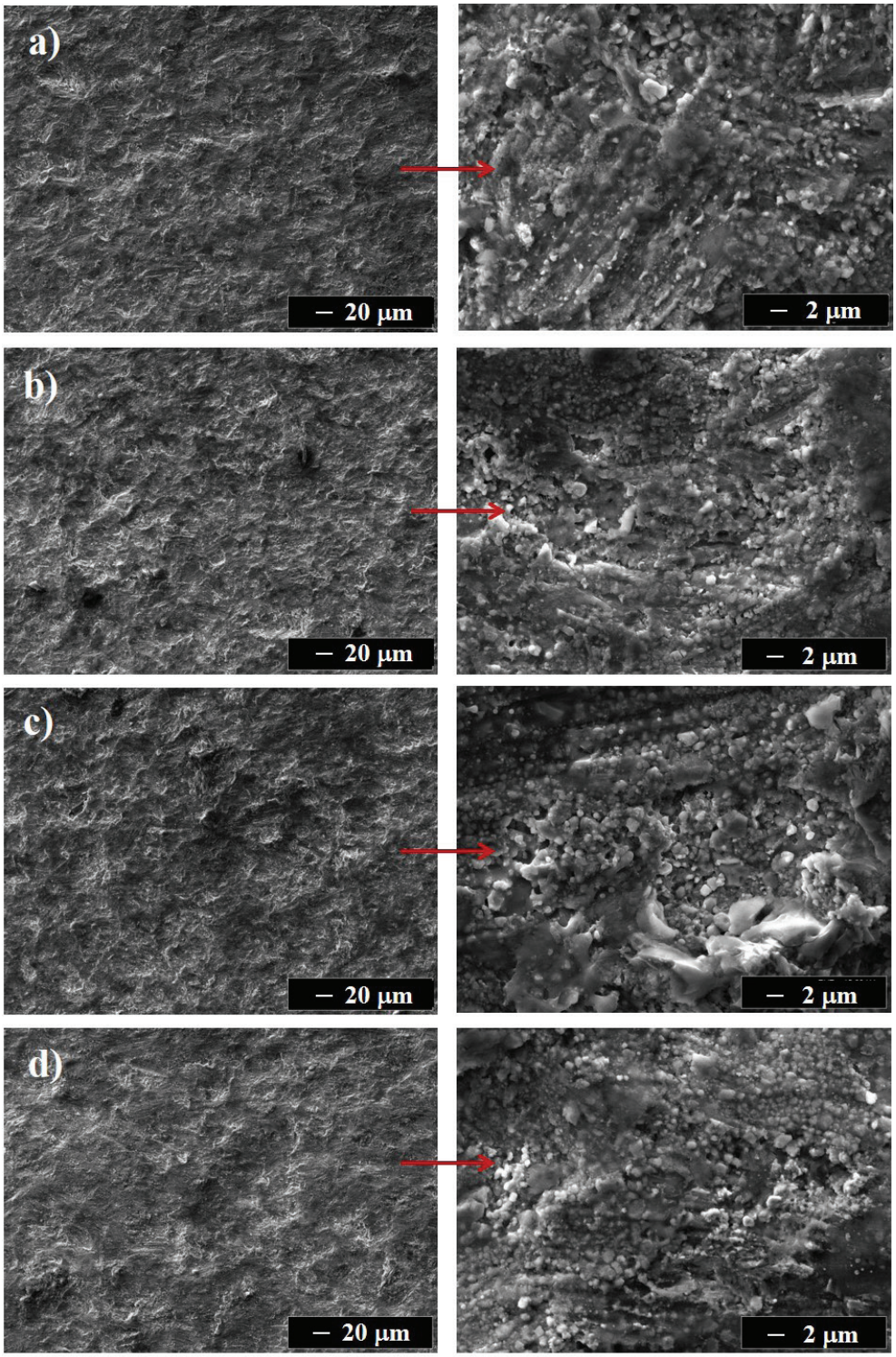

Figure 12. Appearance of damaged surface of specimens after cavitation erosion testing for 60 min.

spark plasma sintering (SPS) at relatively low temperatures of 1250-1350 °C at pressure of 50 MPa. The material with the lowest content of silicon (~30wt.%) sintered at 1350 °C temperature and applied pressure of 50 MPa demonstrated the hardness value of ~10.5 GPa and the least wear rate after erosion by silica sand in the temperature interval of 20-650 °C.

Acknowledgment

This work was supported by the Mobilitas Pluss Postdoctoral Researcher Grant project MOBJD166 (S. Aydinyan) and the Estonia Research Council under PUT1063 (I. Hussainova).

References

[1] E.S. Kang, D.I. Chungand, Y.K. Paek, The Effects of Sintering Aids on the Sintering Behaviour of TiB_2-based Ceramics, Ceramic Armor Material Conference, (1990) 25-44.

[2] R.Z. Yuan, Z.Y. Fu, Z.A. Munir, X.X. Zhou, Z.L. Yang, Fabrication of Dense TiB_2-Al Composites by the Self-propagating High-temperature Synthesis(SHS) Method, J. Mater. Synth. Proc. 1 (3) (1993) 153-57.

[3] H.B. Lee, S.H. Kim, S.W. Kang, Y.H. Han, Characterisation of Mechanically Alloyed Ti-Al-B Nanocomposite Consolidated by Spark Plasma Sintering, Br Ceram. Trans. J. 102 (6) (2003) 231-36.

[4] H.B. Lee, I.J. Kwon, H.J. Lee, Y.H. Han, Characterization of Mechanical Alloying Processed Ti-Si-B Nanocomposite Consolidated by Spark Plasma Sintering, J. Korean Ceram. Soc. 45(12) (2008), 815-820.
[5] G.S. Gan, L. Zhang, Y. Lu, B. Yang, Microstructure and thermo-physical properties of TiB_2/Si-30Al composite for electronic packaging applications, Int. Mater. Sci. Forum. 687 (2011) 138-143.
[6] M. Ohyanagi, T. Tsujikami, S. Sugahara, M. Koizumi, E.A. Levashov, I.P. Borovinskaya, Graded material of diamond dispersed TiB_2-Si composite by SHS/dynamic pseudo isostatic compaction, Int. Mater. Sci. Forum. 308 (1999), 145-150.
[7] P.K.P. Rupa, P.C. Chakraborti, S.K. Mishra, Mechanical and deformation behaviour of titanium diboride thin films deposited by magnetron sputtering, Thin Solid Films, 517(9) (2009) 2912-2919.
[8] B. Basu, G.B. Raju, A.K. Suri, Processing and properties of monolithic TiB_2 based materials, Int. Mater. Rev. 51(6) (2006) 352-374.
[9] L. Lu, M.O. Lai, H.Y. Wang, Synthesis of titanium diboride TiB_2 and Ti-Al-B metal matrix composites, J. Mater. Sci. 35(1) (2000) 241-248.
[10] W. Wang, Z. Fu, H. Wang, R.Yuan, Influence of hot pressing sintering temperature and time on microstructure and mechanical properties of TiB_2 ceramics, J. Eur. Ceram. Soc. 22(7) (2002) 1045-1049.
[11] R. Königshofer, S. Furnsinn, P. Steinkellner, W. Lengauer, R. Haas, K. Rabitsch, Solid-state properties of hot-pressed TiB_2 ceramics, Int. J. Refract. Met Hard Mater. 23 (2005) 350-357.
[12] Y.S. Kang, S.H. Kang, D.J. Kim, Effect of addition of Cr on the sintering of TiB_2 ceramics, J. Mater. Sci. 40 (15) (2005) 4153-4155.
[13] Y. Zhang, N. Ma, H. Wang, Y. Le, X. Li, Damping capacity of in situ TiB_2 particulates reinforced aluminium composites with Ti addition, Mater. Design. 28(2) (2007) 628-632.
[14] T. Fan, G. Yang, D. Zhang, Thermodynamic effect of alloying addition on in-situ reinforced TiB_2/Al composites, Metal. Mater. Trans. A, 36 (1) (2005) 225-33.
[15] H.M. Rajan, S. Ramabalan, I. Dinaharan, S.J. Vijay, Synthesis and characterization of in situ formed titanium diboride particulate reinforced AA7075 aluminum alloy cast composites, Mater. Design. 44 (2013) 438-45.
[16] B. Li, Y. Liu, H. Cao, L. He, J. Li, Rapid synthesis of TiB_2/Fe composite in situ by spark plasma sintering, J. Mater. Sci. 44 (2009) 3909-12.
[17] A. Anal, T.K. Bandyopadhyay, K. Das, Synthesis and characterization of TiB_2-reinforced iron-based composites, J. Mater. Proc. Technol. 172 (2006) 70-76.
[18] M. Ziemnicka-Sylwester, Superhard TiB_2-based composites with different matrix fabricated from elemental powders by SHS-p-HIP, Adv. Sci. Technol. 77 (2013) 146-52.
[19] A.K. Khanra, M.M. Godkhindi, L.C. Pathak, Comparative Studies on Sintering Behavior of Self-propagating High-temperature Synthesized Ultra-fine Titanium Diboride Powder, J. Am. Ceram. Soc. 88 (6) (2005) 1619-1621.
[20] M.S. Asl, Z. Ahmadi, S. Parvizi, Z. Balak, I. Farahbakhsh, Contribution of SiC particle size and spark plasma sintering conditions on grain growth and hardness of TiB_2 composites, Ceram. Int. 43(16) (2017) 13924-13931.
[21] A. Li, Y. Zhen, Q. Yin, L. Ma, Y. Yin, Microstructure and properties of (SiC, TiB_2)/B_4C composites by reaction hot pressing, Ceram. Int. 32(8) (2006) 849-856.
[22] Y. Sun, Q. Meng, D. Jia, L. Huang, Influence of titanium diboride on the microstructure and mechanical properties of silicon nitride ceramic, Mater. Lett. 58(14) (2004) 2057-2060.
[23] A.H. Jones, R.S. Dobedoe, M.H. Lewis, Mechanical properties and tribology of Si_3N_4-TiB_2 ceramic composites produced by hot pressing and hot isostatic pressing, J. Eur. Ceram. Soc. 21(7) 2001 969-980.
[24] A. Nozari, S. Heshmati-Manesh, A.Ataie, A facile synthesis of TiB_2nano-particles via mechano-thermal route, Int. J. Refract. Metals. Hard. Mater. 33 (2012) 107-112.
[25] A.G. Merzhanov, History and recent developments in SHS, Ceram. Int. 21(5) (1995) 371-379.
[26] A. Varma, A.S. Rogachev, A.S. Mukasyan, S. Hwang, Combustion synthesis of advanced materials: principles and applications, Adv. Chem. Eng. 24 (1998) 79-226.
[27] G. Zhao, I. Hussainova, M. Antonov, Q. Wang, T. Wang, D-L. Yung, Effect of temperature on the tribological properties of the polyimide composites reinforced with different fibers in sliding and erosive conditions, Tribol. Int. 82 (2015) 525-533.
[28] I. Hussainova, M. Antonov, A. Zikin, Erosive wear of advanced composites based on WC, Tribol. Int. 46 (2012) 254-260.
[29] M. Antonov, R. Veinthal, D-L. Yung, D. Katusin, I. Hussainova, Mapping of impact-abrasive wear performance of WC-Co cemented carbides, Wear 332 (2015) 971-978.
[30] A.A. Shiryaev, Thermodynamics of SHS processes: An advanced approach, Int. J. SHS 4 (1995) 351-362.
[31] W.Tian, H. Kita, H. Hyuga, N. Kondo, Synthesis, microstructure and mechanical properties of reaction-infiltrated TiB_2-SiC-Si composites, J. Alloy Compd., 509(5) (2011) 1819-1823.
[32] I. Hussainova, N. Voltšihhin, E. Cura, S-P. Hannula, Densification and characterization of spark plasma sintered ZrC-ZrO_2 composites, Mater. Sci. Eng. A, 597 (2014), 75-81.
[33] D. Lafatzis, K. Mergia, Oxidation behaviour of Si wafer substrates in air, J. Appl. Phy. 114(14) (2013) 144308.
[34] Z.Q. Yan, X. Xiong, P. Xiao, F. Chen, H.B. Zhang, B.Y. Huang, Si-Mo-SiO_2 oxidation protective coatings prepared by slurry painting for C/C-SiC composites, Surf. Coat. Tech. 202(19) (2008) 4734-4740.